International Journal of Fracture **110:** 325–349, 2001.

Interface cracks in layered materials subjected to a uniform temperature change

F.G. GAUDETTE[1], A.E. GIANNAKOPOULOS[2] and S. SURESH[2]
[1]*Engineering Mechanics Laboratory, General Electric: Corporate Research and Development, Schenectady, NY 12301, USA*
[2]*Department of Materials Science and Engineering, MIT, Cambridge, MA 02139, USA*

Received 2 March 2000; accepted in revised form 11 January 2001

Abstract. Elastic and incremental elasto-plastic analyses have been used to evaluate the driving force for interface edge-crack growth initiation in tri-layered material systems subjected to a monotonic variation in temperature. Whenever possible, closed-form solutions are derived as functions of the thermo-mechanical material properties and the geometry of the layers. Analytical expressions for the different critical temperatures at which distinct transitions occur in thermally induced deformation are presented and are correlated with the three regimes of interface fracture; elastic, partially plastic and fully plastic. Furthermore, a large-scale contact model, which predicts the shielding effect of contact in the wake of an interface crack, is also presented and the attendant reduction in the energy release rate is estimated. Finite element results, showing the influence of layer geometry and strain hardening on the energy release rate, are presented for a model Al_2O_3/Ni(Cr)/Al_2O_3 tri-layered system; these simulations confirm the bounds predicted by the theory.

Key words: Elastoplastic analysis and contact, interface cracks, layered structures.

1. Introduction

When layers of dissimilar materials are bonded, differences in the thermal expansion coefficients, combined with a change in temperature $|\Delta T|$ relative to the stress-free state, result in thermal stresses (Suresh et al., 1994; Shen and Suresh, 1995). These stresses, along with the singular nature of free edges (Bogy, 1971; Kuo, 1989; Cao et al., 1988; He and Evans, 1991) or manufacturing-related edge flaws, can result in the development of interface cracks. When these cracks form, the driving force for crack growth initiation depends on the magnitude of stress in each layer. For small $|\Delta T|$ all the layers in the composite are nominally elastic. Under these circumstances, stress is quantified by elastic and thermal expansion mismatch and $|\Delta T|$, and the driving force for interface fracture is the energy release rate G (Suo and Hutchinson, 1990; Hutchinson and Lu, 1995; Beuth and Narayan, 1996). As $|\Delta T|$ increases, a point is reached at which nominal thermal stresses in the layers exceed the elastic limits of the materials. At this point an elasto-plastic analysis is needed. Interface fracture then has to be predicated upon a different measure of crack driving force, such as the J-integral (Olsson and Giannakopoulos, 1997).

The analytical and numerical study presented below is intended to elucidate the fracture mechanics of edge-cracks in a three-layered material system (tri-layer) having sharp interfaces and subjected to a monotonic temperature change. This type of loading and geometry is typical of diffusion-bonded solids or of thermal-barrier/wear-resistant coatings (Gaudette, 1999).

For both these examples, the tri-layer is stress free at an elevated processing temperature but develops thermal stresses upon cooling.

The purpose of the analysis presented in this paper was to provide a theoretical basis for estimating the bounds for the crack driving force in layered specimens that are bonded and then cooled to room temperature.

2. Problem formulation and material model

For the present work, only metal-ceramic layered systems are studied. This restriction has been imposed to limit the scope. However, the methodology presented is equally applicable to metal–metal and ceramic–ceramic systems. The materials are modeled as isotropic, elastic, or elastic-perfectly plastic, and their plastic response is described by the rate-independent J_2-flow theory. All inelastic deformation is attributed to conventional metal plasticity; creep is not considered. Except for the crack, the materials are assumed to be perfectly bonded, and the crack is assumed to be stationary. If slip between layers, large deformation or material orthotropy are of interest to the reader, the paper by (Di Sciuva et al., 1999) gives ample information to start. Because the problem is formulated as quasi-static, inertia and body forces are ignored. Thermal gradients or transient thermal response are not considered and the instantaneous temperature is taken to be uniform.

The thickness of each layer (H, h, and t from Figure 1) is assumed to be significantly larger than the dimensions of microstructural features such as grain size. The crack length, a, and the ligament ahead of the crack tip, w, must satisfy the condition that $a, w > (H + t + h)$, in order to neglect edge effects. Under these circumstances any dependence of the energy release rate on the crack length is eliminated.

A state of plane stress is considered. The actual three-dimensional thermal stresses affect the plane stress solutions near the interface over a distance comparable to the layer thickness, as has been shown from three-dimensional elastic calculations (Nakamura, 1991). Nevertheless, a plane stress model captures the essential features of the elasto-plastic deformation. Under elastic conditions, plane stress results can be carried over for the plane strain state by replacing the elastic modulus, E, and the coefficient of thermal expansion, α, of each layer with $E/(1-\nu^2)$ and $\alpha(1+\nu)$ respectively (Suresh et al., 1994). Small strain kinematics are assumed, with the total strain being decomposed into the elastic, plastic, and thermal parts, $\varepsilon_{ij} = \varepsilon_{ij}^{\text{elastic}} + \varepsilon_{ij}^{\text{plastic}} + \varepsilon_{ij}^{\text{thermal}}$, respectively.

The properties and field quantities for the metal layer are denoted by the subscript 2. All materials are assumed to be stress free at zero initial temperature. It is sufficiently general to model layers 1 and 3 as isotropic and linear elastic with Young's moduli E_1 and E_3, respectively. This assumption is consistent with the diffusion bonded Al_2O_3/ Ni(Cr)/Al_2O_3 tri-layer (Gaudette et al., 1997). It is also consistent with a thermal-barrier coating deposited on a high yield strength substrate, i.e., a Waspaloy substrate with a deposited NiCrAlY bond coat and protective ceramic coating (Gaudette, 1999). For the purposes of obtaining closed-form solutions, the properties of all layers are assumed to be independent of temperature; however, a similar methodology can be used for layers with temperature dependent properties.

The paper is arranged as follows. In Section 3, elastic stress analysis is used along with the J-integral to derive an expression for the elastic interface energy release rate. This result is then tailored for Cases A and B, Section 4. In Section 5 an interface contact model is presented. The model predicts the shielding effect associated with large- scale elastic contact in the wake

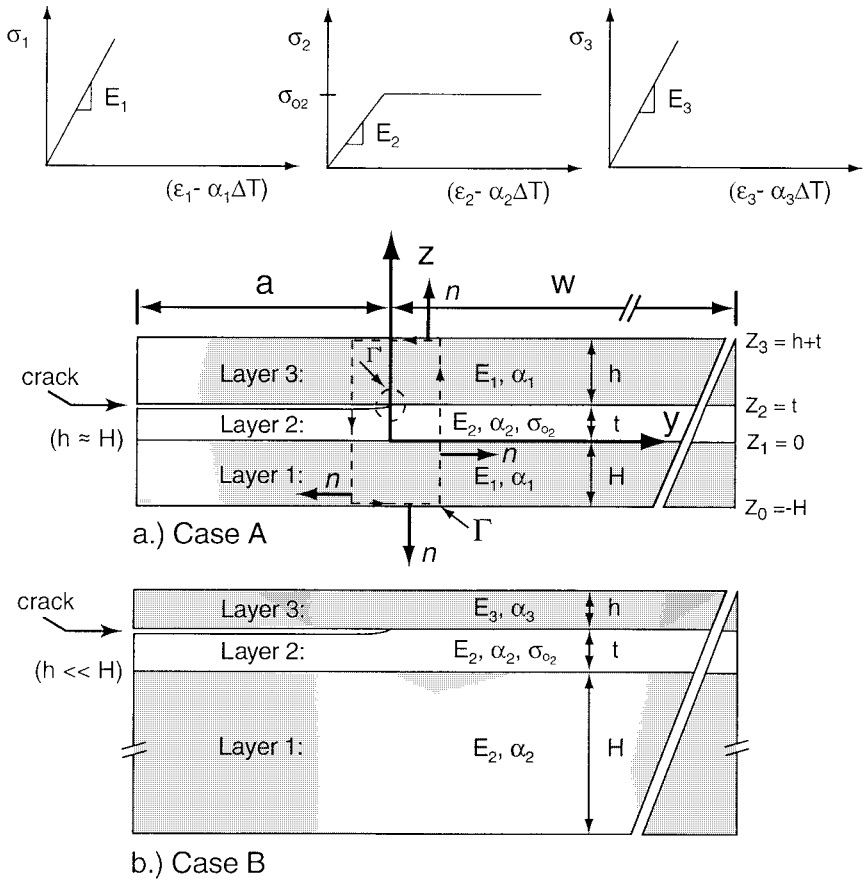

Figure 1. Configurations considered for analysis: Case A, a diffusion-bonded tri-layer, and Case B, a thermal-barrier/wear-resistant coating. The far-field and near-tip contours Γ and Γ' are shown respectively.

of an interface crack. Section 6 contains analytical plasticity derivations, including those for characteristic temperature changes required for the onset of yielding in layer 2 and for it to yield completely. Expressions for the limiting elastic energy release rate, related to the former temperature change, are given in Section 7.

Since the analysis for a three-layered material requires an understanding of the stress development in the bi-layer comprising the crack wake and the tri-layer ahead of the crack tip, a discussion of the plastic yielding sequence is presented. The results establish important bounds on the elasto-plastic crack driving force, the J-integral, for tri-layers as discussed in Section 8. Sections 9 and 10 present and discuss finite element results for the Al_2O_3/Ni(Cr)/Al_2O_3 tri-layer. Included are the normal and shear stress distributions, close to and ahead of, the crack-tip.

3. Elastic analytical results

3.1. Elastic interface energy release rate G

The elastic interface energy release rate, G, for a general three-layered material is presented first. The coordinate system is located such that the y-direction is parallel to and on the layer 1/layer 2 interface (henceforth referred to as the 1–2 interface). The z-direction is normal to the 1–2 interface at a position such that $y = 0$ corresponds to the location of the crack tip as indicated in Figure 1. The method for obtaining G is analogous to evaluating the J-integral along the contour Γ depicted in Figure 1 (Suo and Hutchinson, 1990).

$$J = \int_{\Gamma} \left(\left(\int \sigma_{ij} \, \mathrm{d}\varepsilon_{ij} \right) \mathrm{d}z - \sigma_{ij} \eta_j \frac{\partial u}{\partial y} \mathrm{d}\Gamma \right) + \iint_{A} \sigma_{ij} \frac{\partial \varepsilon_{ij}^{T}}{\partial y} \, \mathrm{d}A \, . \tag{3.1}$$

In Equation (3.1) ε_{ij}^{T}, σ_{ij}, n_j, and u_i are the thermal strain tensor, the stress tensor, the vector normal to the contour Γ, and the displacement vector, respectively. A is the area enclosed by Γ. When $\partial \varepsilon_{ij}^{T} / \partial y = 0$, that is for homogeneous thermal strain variations along the crack direction, the J-integral is path independent and therefore $J = G$.

3.2. Stress analysis and elastic strain energy

Far ahead of the crack the three layered system behaves elastically for small ΔT. For plane stress the stress-strain relationship for each layer is given by:

$$\sigma_{yy_{1,2,3}}(z) = E_{1,2,3} \left(\varepsilon_o + \kappa z - \alpha_{1,2,3} \Delta T \right) \, , \tag{3.2}$$

where $E, \alpha, \Delta T, \varepsilon_o$, and κ are the Young's modulus, the coefficient of thermal expansion, the temperature change relative to a stress free state, the strain at the 1–2 interface and the curvature, respectively. The subscripts 1, 2, or 3 refer to the layer number.

By substituting Equation (3.2) into the force and moment equilibrium equations, Equations (3.3) and (3.4), respectively,

$$\int_{-H}^{0} \sigma_{yy_1}(z) \, \mathrm{d}z + \int_{0}^{t} \sigma_{yy_2}(z) \, \mathrm{d}z + \int_{t}^{h+t} \sigma_{yy_3}(z) \, \mathrm{d}z = 0 \tag{3.3}$$

$$\int_{-H}^{0} \sigma_{yy_1}(z) z \, \mathrm{d}z + \int_{0}^{t} \sigma_{yy_2}(z) z \, \mathrm{d}z + \int_{t}^{h+t} \sigma_{yy_3}(z) z \, \mathrm{d}z = 0 \, , \tag{3.4}$$

equations for the strain, ε_o and the curvature, κ, far ahead of the crack tip can be obtained,

$$\varepsilon_0 = \alpha_2 \Delta T \left(\frac{4\lambda_3\lambda_4 - 3\lambda_2\lambda_5}{4\lambda_1\lambda_3 - 3\lambda_2^2} \right) \, , \qquad \kappa = \frac{6\alpha_2 \Delta T}{t} \left(\frac{\lambda_1\lambda_5 - \lambda_2\lambda_4}{4\lambda_1\lambda_3 - 3\lambda_2^2} \right) \, . \tag{3.5}$$

The dimensionless variables used in these equations are defined as:

$$\lambda_1 = X\varsigma + Z\eta + 1, \quad \lambda_2 = -X\varsigma^2 + Z\left((\eta+1)^2 - 1\right) + 1 \, ,$$

$$\lambda_3 = X\varsigma^3 + Z\left((\eta+1)^3 - 1\right) + 1, \quad \lambda_4 = XY\varsigma + ZW\eta + 1 \, ,$$

$$\lambda_5 = -XY\varsigma^2 + ZW\left((\eta+1)^2 - 1\right) + 1 \, , \tag{3.6}$$

$$\eta = h/t, \quad \varsigma = H/t, \quad \theta = (\varsigma + 1)/\eta, \quad X = E_1/E_2, \quad Z = E_3/E_2 ,$$

$$Y = \alpha_1/\alpha_2, \quad W = \alpha_3/\alpha_2 .$$

By substituting Equation (3.5) into Equation (3.2), the stress distribution in each layer can be obtained and then,

$$\overline{U} = \frac{U}{ab} = \frac{1}{2}\sum_{i=1}^{3}\int_{Z_{i-1}}^{Z_i} \frac{(\sigma_{yy_i}(z))^2}{E_i}\mathrm{d}z \tag{3.7}$$

gives the total elastic strain energy stored in the tri-layer far ahead of the crack tip. Equation (3.7) is the elastic strain energy normalized by the in-plane area (ab), where b is the specimen width and a is the crack length.

When an interface crack is located between layers 2 and 3, the tri-layer behaves as a perfectly bonded bi-layer with layers 1 and 2 ($z < t$) and a homogeneous layer 3 ($z > t$). Since both parts of the tri-layer experience the same ΔT, the bi-layer has its own strain, ε_o, and curvature, κ. In the absence of contact for $y < 0$, ε_o and κ for the bi-layer can be obtained from Equation (3.5) by setting $\eta = h/t = 0$:

$$\frac{\varepsilon_0 - \alpha_2\Delta T}{\Delta T(\alpha_2 - \alpha_1)} = \frac{-X\varsigma(X\varsigma^3 + 3\varsigma + 4)}{\xi}\ (\mathrm{bi-layer}) , \tag{3.8}$$

$$\frac{\kappa t}{\Delta T(\alpha_2 - \alpha_1)} = \frac{6X\varsigma(\varsigma + 1)}{\xi}\ (\mathrm{bi-layer}) , \tag{3.9}$$

where $\xi = X\varsigma(X\varsigma^3 + 4\varsigma^2 + 6\varsigma + 4) + 1$. Layer 3 is stress free behind the crack tip so that $\varepsilon_0 = \alpha_3\Delta T, \kappa = 0$. When Equations (3.8) and (3.9) are substituted into Equation (3.2) the equilibrium stress state in the bi-layer is obtained. Further substitution into Equation (3.7) gives the normalized elastic strain energy, $\overline{U}^*$, stored in the wake of the interface crack.

In the absence of external work, the elastic interface energy release rate is a result of two processes: the release of all elastic strain energy in layer 3 and a redistribution of stress resulting from the transition from a tri-layer for $y > 0$ to a bi-layer for $y < 0$. The elastic interface energy release rate is given by

$$J = G = \overline{U} - \overline{U}^* . \tag{3.10}$$

4. The energy release rate G: Cases A and B

If additional assumptions regarding the material properties of layers 1–3 are made, then Equations (3.5)–(3.9) can be simplified to yield compact expressions for G. Cases A and B are based on two sets of assumptions. For Case A, layers 1 and 3 are elastic and have the same material properties while layer 2 is elastic-perfectly plastic. For Case B layers 1 and 3 are elastic and layers 1 and 2 have the same elastic properties; yet layer 2 is elastic-perfectly plastic (typical of a thermal barrier coating with low yield strength bond coat). The purely elastic response for each case is examined first.

For Case A, $Z = X$ and $W = Y$; thus, λ_1, λ_2, and λ_3 simplify to $\lambda_1^A = X(\eta+\varsigma)+1$, $\lambda_2^A = X(\eta^2 - \varsigma^2 + 2\eta) + 1$, and $\lambda_3^A = X((\eta + 1)^3 + \varsigma^3 - 1) + 1$. Making these substitutions along with those for λ_4 and λ_5 into Equation (3.5), we obtain expressions for ε_o, and κ:

$$\frac{\varepsilon_0^A - \alpha_2 \Delta T}{\Delta T(\alpha_1 - \alpha_2)} = \frac{2X^2\varsigma\eta\left(2(\eta+\varsigma)^2 + 6(\eta+\varsigma+1) - \varsigma\eta\right) + X^2(\eta^4+\varsigma^4)}{4\lambda_1^A\lambda_3^A - 3(\lambda_2^A)^2}$$

$$+\frac{3X(\varsigma^2-\eta^2) + 2X(2\varsigma-\eta)}{4\lambda_1^A\lambda_3^A - 3(\lambda_2^A)^2} = C_1\,, \tag{4.1}$$

$$\frac{\kappa^A t}{\Delta T(\alpha_1-\alpha_2)} = \frac{6X(\eta^2+\eta-(\varsigma^2+\varsigma))}{4\lambda_1^A\lambda_3^A - 3(\lambda_2^A)^2} = C_2\,.$$

These equations have been non-dimensionalized to arrange the material properties and loading on the left-hand side, and the moduli and geometric ratios on the right-hand side. The superscript A indicates Case A. Substituting Equation (4.1) into Equations (3.2) and (3.7) provides the normalized elastic strain energy, $\overline{U}^A$, ahead of the crack:

$$\overline{U}^A = \frac{1}{6E_2t(\Delta T(\alpha_2-\alpha_1))^2}\left(X\varsigma\left(3(C_1-1)^2 - 3C_2\varsigma(C_1-1) + (C_2\varsigma\right)^2\right) + \tag{4.2}$$
$$\left(3C_1^2 + 3C_1C_2 + C_2^2\right) + X\eta\left(3(C_1-1+C_2)^2 + 3C_2\eta(C_1-1+C_2) + (C_2\eta)^2\right)\Big)\,.$$

Setting $\eta = h/t = 0$ in Equations (4.1) and (4.2), the normalized elastic strain energy for the bi-layer, $\overline{U}^{*A}$, in the crack wake (Suo, 1990; Olsson, 1997) is

$$\frac{\overline{U}^{*A}}{E_2t(\Delta T(\alpha_2-\alpha_1))^2} = \frac{X\varsigma(X\varsigma^3+1)}{2\xi}\,. \tag{4.3}$$

When $h = H$, there is both material and geometric symmetry. As a result, $\varsigma = \eta$ and the (normalized) interface energy release rate simplifies to:

$$\frac{G^A}{E_2t(\Delta T(\alpha_2-\alpha_1))^2} = \frac{X\eta}{2(2X\eta+1)}\left(\frac{X\eta^2(7\eta+12)+6X\eta+1}{\xi'}\right)\,, \tag{4.4}$$

where $\xi' = X\eta(X\eta^3+4\eta^2+6\eta+4)+1$.

For Case B, $X = 1$ and $Y = 1$. Thus, when layers 1 and 2 have the same elastic properties, the tri-layer problem converges to the bi-layer problem. By making the substitutions $X = (1/Z)$, $\varsigma \to \theta = (\varsigma+1)/\eta$, $E_2 \to E_3$, $E_1 \to E_2$, $\alpha_2 \to \alpha_3$, $\alpha_1 \to \alpha_2$, and $t = h$ into Equations (3.8), (3.9), and (4.3) we obtain:

$$\frac{\varepsilon_0^B - \alpha_3\Delta T}{\Delta T(\alpha_3-\alpha_2)} = \frac{-\theta\left((\theta^3/Z)+3\theta+4\right)}{\theta^2\left((\theta^2/Z)+4\theta+6\right)+4\theta+Z}\,,$$
$$\frac{\kappa^B h}{\Delta T(\alpha_3-\alpha_2)} = \frac{6\theta(\theta+1)}{\theta^2\left((\theta^2/Z)+4\theta+6\right)+4\theta+Z}\,. \tag{4.5}$$

The superscript B indicates Case B. The resulting equation for the interface energy release rate is then:

$$\frac{G^B}{E_3h(\Delta T(\alpha_3-\alpha_2))^2} = \frac{1}{2}\frac{\theta\left((\theta^3/Z)+1\right)}{(\theta^4/Z)+\theta(4\theta^2+6\theta+4)+Z}\,. \tag{4.6}$$

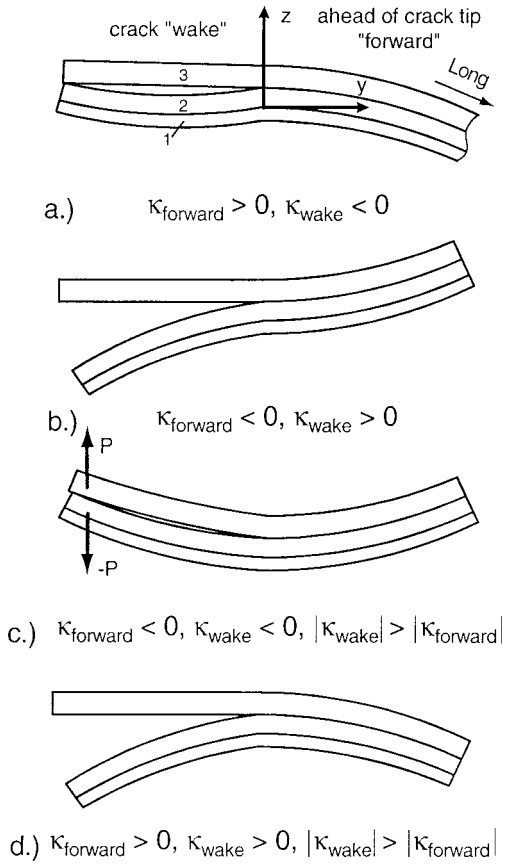

Figure 2. Modes of deformation during interface fracture in the three layered system. (a) and (c) illustrate the conditions when large-scale contact must be accounted for. (b) and (d) illustrate the conditions when there is no large-scale contact.

5. Interfacial contact

Equations (3.10), (4.4) and (4.6) assume there is no contact in the wake of the crack. For the general three-layered system there are four possible modes of deformation. These modes are shown in Figure 2. Figures 2a and 2c represent the two possible scenarios for large-scale contact. In both instances, the unconstrained curvature of the bi-layer along the crack wake is negative. This leads to the criterion $\Delta T(\alpha_2 - \alpha_1) < 0$ for contact.

For Case B, layers 1 and 2 are elastically matched ($E_1 = E_2$, and $\alpha_1 = \alpha_2$). As a result, the curvature in the wake of the crack is zero. Furthermore, the substrate, layer 1, for thermal-barrier/wear-resistant coatings is substantially thicker than the other layers; thus there would be negligible curvature ahead of the crack tip. Considering both of these conditions, Case B would never experience large-scale contact in the crack wake. However, the same is not true for Case A.

When contact occurs, the bi-layer is subjected to a superimposed mechanical stress distribution and layer 3 is no longer stress free. This results in accumulation of elastic strain energy in the wake, causing Equation (4.4) to overestimate G. If we assume that the contact is frictionless and that the stress distributions in layers 1–3 under these circumstances vary

only in the y and z directions, then an estimate of the 'shielding effect' due to contact can be obtained. By virtual work, the difference between the actual energy release rate, $G_{(\text{contact})}$, and the energy release rate without contact, $G_{(\text{no contact})}$, is given by:[1]

$$\Delta G = G_{(\text{no contact})} - G_{(\text{contact})} = \sum_{i=1}^{3} \frac{E_i}{a} \int_0^a \int_{Z_{i-1}}^{Z_i} \Delta\varepsilon^2_{yy_{i(\text{mech})}}(y, z)\, \mathrm{d}z\, \mathrm{d}y\ , \tag{5.1}$$

where $\Delta\varepsilon_{yy_{i(\text{mech})}}$ is the change in strain distribution for layer i due to the superimposed mechanical loads associated with contact constraint.

In order to estimate Equation (5.1), a simple contact model has been created as shown in Figure 2. The model is based on the assumption that frictionless contact takes place at the end of the crack at $y = -a$ and that the contact force per unit width, P, results in curvature compatibility between layers 1–3 at $y = 0$. Since equilibrium requires the contact force on the bi-layer and layer 3 to be equal and opposite, the net effect of P is to decrease the negative curvature of the bi-layer while creating the same curvature in layer 3. Using beam theory and neglecting work from shear forces we obtain:

$$\kappa + \frac{Pa}{\overline{EI}} = -\frac{12Pa}{E_3 h^3}\ , \tag{5.2}$$

where $\overline{EI}$ is the mechanical flexural stiffness of the bi-layer, which relates the curvature due to the mechanical moment per unit width, and for an orthogonal cross-section.

$$\overline{EI} = \frac{E_2 t^3}{12(X\varsigma + 1)}\xi\ . \tag{5.3}$$

When Equations (3.9) and (5.3) are substituted into Equation (5.2), an expression for the contact force per unit width is obtained:

$$P = \frac{\Delta T(\alpha_1 - \alpha_2)E_3 t^2}{2a} \frac{X\eta^3\varsigma(\varsigma + 1)}{\left(Z\eta^3(X\varsigma + 1) + \xi\right)}\ . \tag{5.4}$$

The mechanical bending moment M, associated with P, is a linear function of y varying from 0 at $y = -a$ to Pa ($-Pa$ for layer 3) at $y = 0$. At any given position along the crack length, $M(y) = (a + y)P$, and the mid-plane strain and curvature for the mechanically loaded bi-layer is:

$$\begin{aligned} \varepsilon_{0_{\text{mech}}} &= \frac{6M(\eta^2 X - 1)}{E_2 \xi t^2} = \frac{6P(a + y)(\eta^2 X - 1)}{E_2 \xi t^2}\ , \\ \kappa_{\text{mech}} &= \frac{12M(\eta X + 1)}{E_2 \xi t^3} = \frac{12P(a + y)(\eta^2 X + 1)}{E_2 \xi t^2}\ . \end{aligned} \tag{5.5}$$

Adding these two strain components to those given by Equations (3.8) and (3.9) yields an expression for the total strain in layers 1 and 2:

$$\varepsilon_{1,2} = \varepsilon_{0_{\text{mech}}} + \varepsilon_o + \kappa_{\text{mech}} z + \kappa z - \alpha_{1,2}\Delta T\ . \tag{5.6}$$

Note that the sign convention for the strain components is completely specified by Equations (5.5), (3.8) and (3.9). Substituting the total strain in layers 1 and 2 into Equation (5.1), an expression for the shielding effect is obtained in terms of a decrease in the energy release rate,

[1] This assumption is appropriate as long as $a > 3(H + t)$ and the specimen width $b < 3(H + t)$.

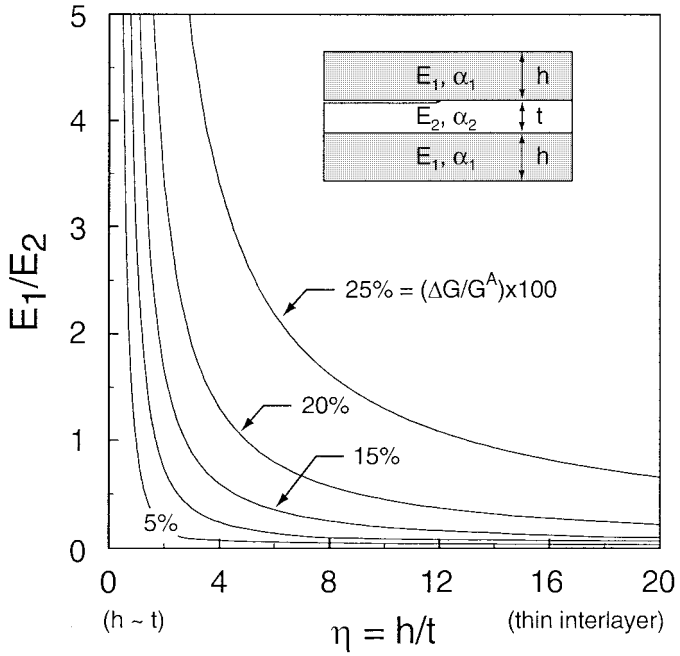

Figure 3. The shielding effect of large-scale contact between the bi-layer at the crack wake and layer 3 for Case A with $H = h$.

$$\Delta G = \sum_{i=1}^{2} \frac{E_i}{a} \int_{-a}^{0} \int_{Z_{i-1}}^{Z_i} \varepsilon_i^2 \, \mathrm{d}z \, \mathrm{d}y + \frac{E_3}{a} \int_{-a}^{0} \int_{-h/2}^{h/2} \left(\frac{12M(y)z}{E_3 h^3} \right) \mathrm{d}z \, \mathrm{d}y - 2\overline{U}^{*A} \,. \tag{5.7}$$

Figure 3 contains a plot of ΔG, for $H = h$, normalized by G^A given by Equation (4.4). The contours show the shielding effect as a percentage of the no-contact energy release rate. As defined, this percentage represents the reduction in energy release rate resulting from contact. It is interesting to note that this ratio does not depend on ΔT, α's, the crack length or any individual thickness parameter. For the range of E_1/E_2 and η shown in Figure 3, $\Delta G/G^A$ can be approximated by:

$$\frac{\Delta G}{G^A} = \frac{2X^2\eta^4(\eta+1)^2(2X\eta+1)}{(7X\eta^3+12X\eta^2+6X\eta+1)+(2X^2\eta^4+5X\eta^3+6X\eta^2+4\eta+1)} \,. \tag{5.8}$$

6. Analytical results for the onset of yielding

The preceding derivations assumed elastic material response. Since most materials have a well defined elastic limit, this assumption breaks down once a critical temperature change is reached. For metals with yield strength, σ_{oi}; $i = 1$–3, the limits of elasticity are reached when yielding within any of the three layers begins for the first time (here, far-field yielding is the criterion used for judging the limits of elasticity for the layered beams). Beyond this point, fracture is characterized better by the J-integral rather than the elastic interface energy release rate, G.

Determining the critical temperature change, referred to as $|\Delta T_{\text{onset}}|$, requires that the absolute value of the maximum effective stress in each layer be compared with its yield strength.

In the plane stress case, the yield condition is $|\sigma_{yyi}| = |\sigma_{oi}|$, $i = 1$–3. Since this always occurs at the end of the layer, i.e. at positions z_i as indicated in Figure 1, $|\Delta T_{\text{onset}}|$ is equal to the minimum of all $|\Delta T|$ required to yield at least one of the layers 1, 2, or 3 at the positions z_i, in either the tri-layer far ahead of the crack tip or the bi-layer in the crack wake.

For Case A with $E_1 = E_3$ and layers 1 and 3 elastic, yielding always begins in layer 2 at either the 2–3 or the 1–2 interface (for the bi-layer, the 2–3 interface refers to the free surface of layer 2 between layers 2 and 3). Making the appropriate substitutions, the temperature changes at which yielding begins at these locations are given by:

$$\frac{E_2|\Delta T^A_{2-3}(\alpha_1 - \alpha_2)|}{\sigma_{o2}} = \frac{1}{C_1 + C_2} \tag{6.1}$$

and

$$\frac{E_2|\Delta T^A_{1-2}(\alpha_1 - \alpha_2)|}{\sigma_{o2}} = \frac{1}{C_1}, \tag{6.2}$$

respectively. C_1 and C_2 have been defined in Equation (4.1) and σ_{o2} is the yield strength of the second layer. Equations (6.1) and (6.2) are also valid for the bi-layer when the substitution $\eta = h/t = 0$ is made in C_1 and C_2. Here ΔT^A_{2-3} and ΔT^A_{2-3} are the temperature changes required to start yielding layer 2 at the 1–2 and 2–3 interface respectively. When the thicknesses of layer 1 and 3 are the same, $H = h$, Equations (6.1) and (6.2) give the same value indicating that yielding occurs uniformly through the entire thickness of layer 2 for the tri-layer:

$$\frac{E_2|\Delta T^A_{2-3}(\alpha_1 - \alpha_2)|}{\sigma_{o2}} = \frac{E_2|\Delta T^A_{1-2}(\alpha_1 - \alpha_2)|}{\sigma_{o2}} = \frac{1}{2X\eta} + 1. \tag{6.3}$$

Case A has two important temperature changes which must be compared in order to establish $|\Delta T_{\text{onset}}|$. They are the minimum temperature changes required to start yielding in the tri-layer and in the bi-layer. By comparing Equations (6.1) and (6.2) it can be shown that yielding in the wake bi-layer always begins at the 1–2 interface and that yielding in the tri-layer always begins at the interface adjacent to the thicker of layers 1 and 3. When $h = H$, layer 2 yields uniformly ahead of the crack-tip and yielding in the tri-layer precedes yielding in the bi-layer whenever

$$7X\varsigma^4 + 6X\varsigma^3 - 3\varsigma^2 - 2\varsigma > 0. \tag{6.4}$$

Under these circumstances $|\Delta T_{\text{onset}}| = |\Delta T^A_{1-2}| = |\Delta T^A_{2-3}|$ for the tri-layer. For most metal/ceramic interfaces with $X > 1$ and $\varsigma > 1$, Equation (6.4) is generally satisfied. Problems do, however, arise when $\varsigma = h/t \ll 1$. Under these circumstances, it is possible that yielding precedes in the bi-layer at the 1–2 interface. The present work examines only the cases when Equation (6.4) is satisfied and, therefore, yielding starts ahead of the crack-tip.

For Case B, layer 1 and 2 are elastically matched, therefore, the bi-layer does not yield. Under these circumstances yielding always begins at the interface between layers 2 and 3 in the tri-layer ahead of the crack-tip. The temperature at which this occurs can be found from the bi-layer solution by substituting $E_1 \to E_2, \alpha_1 \to \alpha_1, \alpha_2 \to \alpha_3, \sigma_{o1} \to \sigma_{o2}, X = E_1/E_2 \to 1/Z \to E_2/E_3$ and $\varsigma \to \theta = (\varsigma + 1)/\eta$:

$$\frac{E_2|\Delta T^B_{2-3}(\alpha_3 - \alpha_2)|}{\sigma_{o2}} = \frac{\theta^2\left(\dfrac{\theta^2}{Z} + 4\theta + 6\right) + 4\theta + Z}{3\theta^2 + 4\theta^3 + Z}. \tag{6.5}$$

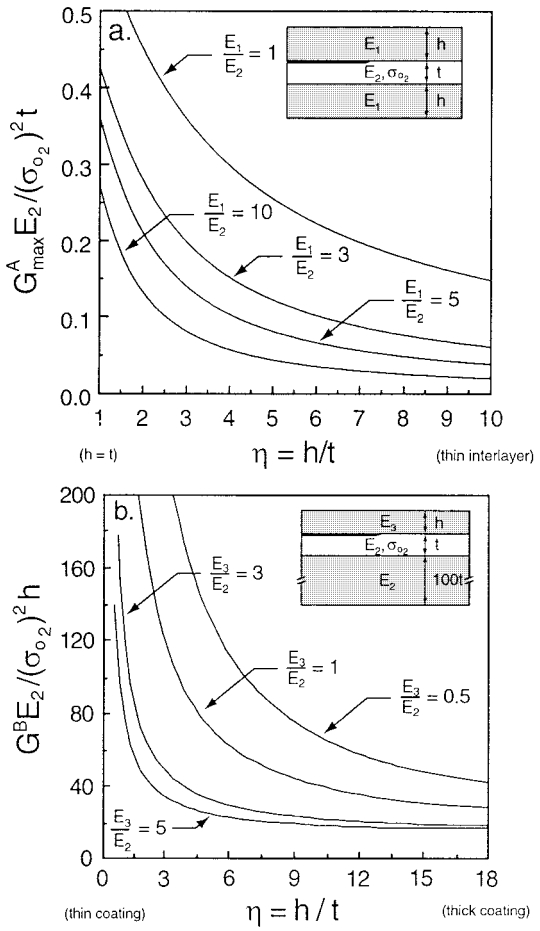

Figure 4. The limit for the elastic interface energy release rate, $G_{\max}$: (a) Case A, with geometric symmetry and (b) Case B, with $H/t = 100$ (typical of thin coatings on a thick substrate).

The critical temperature change $|\Delta T_{\text{onset}}|$ is equal to $|\Delta T^B_{2-3}|$.

7. An upper bound for the energy release rate

By combining $|\Delta T_{\text{onset}}|$ with Equations (3.10), (4.4) and (4.6), upper bounds for the elastic interface energy release rate can be obtained. For Case A with $H = h$, this limit is

$$\frac{G^A E_2}{t(\sigma_{o2})^2} = \frac{2X\eta + 1}{8X\eta} \frac{X\eta^2(7\eta + 12) + 6X\eta + 1}{X\eta(4(\eta + 1)^2 + \eta(X\eta^2 - 2)) + 1}. \tag{7.1}$$

This equation is plotted in Figure 4a for a range of $\varsigma = h/t = H/t = \eta$ and $X = E_1/E_2 = 1, 3, 5$, and 10 (typical Ni/Al_2O_3 and Al/Al_2O_3 interfaces have $E_1/E_2 = 2$ and 6, respectively). Since all ς and X shown in the figure satisfy Equation (6.4), the maximum elastic driving force is achieved just before layer 2 ahead of the crack tip yields uniformly. For further increase in $|\Delta T|$, the J-integral diverges from G due to the presence of plasticity.

For Case B, the upper bound on G can be found by substituting Equation (6.5) into Equation (4.6) which gives:

$$\frac{G^B E_2}{h(\sigma_{o2})^2} = \frac{(\theta^4 + \theta Z)\left(\dfrac{\theta^4}{Z} + \theta(4\theta^2 + 6\theta + 4) + Z\right)}{2(4\theta^3 + 3\theta^2 + Z)^2}\,, \tag{7.2}$$

where $\theta = (H+t)/h$ and $Z = E_3/E_2$. Figure 4b gives a plot of Equation (7.2) for $H = 100t$, typical of thin layers deposited on a thick substrate.

8. Temperatures corresponding to fully plastic layers

Further monotonic temperature change beyond $|\Delta T_{\text{onset}}|$ results in the following[2]: (i) the elasto-plastic boundary propagates through the thickness of layer 2 ahead of the crack (Case A and B), (ii) plasticity begins in layer 2 at the 1–2 interface in the wake of the crack (Case A), and (iii) the elasto-plastic boundary propagates through the thickness of layer 2 in the wake of the crack (Case A). For both (i) and (iii) characteristic temperature changes are reached at which point layer 2 becomes fully plastic.

When layer 2 is elastic-perfectly plastic, analytical expressions for temperatures that result in a fully plastic layer 2 can be obtained. For clarity these $|\Delta T|$ are labeled $|\Delta T_{FP}|$ indicating the temperature change where layer 2 plastifies completely for the first time.

For Case A (Shen and Suresh, 1995), $|\Delta T_{FP}| = |\Delta T^A_{FP}|$:

$$\begin{aligned}
&\frac{E_2|\Delta T^A_{FP}(\alpha_1 - \alpha_2)|}{\sigma_{o2}} = \frac{1}{X\eta}\left(\frac{D^A_1 + D^A_2}{D^A_3 + D^A_4 + D^A_5}\right)\,,\\
&D^A_1 = \tfrac{1}{3}\left(X\eta(\phi+1)+1\right)\left(\eta^2(\phi^3+1) + 3\phi(\eta\phi+1)\right)\,,\\
&D^A_2 = \tfrac{1}{4}\left(\eta(\phi^2-1)+2\phi\right)\left(X\eta\phi(\eta\phi+2) - X\eta^2 + 1\right)\,,\\
&D^A_3 = \tfrac{1}{12}\eta^2(\phi^4+1), \quad D^A_4 = \tfrac{1}{6}\eta^2\phi(2\phi^2+3\phi+2), \quad D^A_5 = \phi(\eta\phi+\eta+1)\,.
\end{aligned} \tag{8.1}$$

In deriving these equations it is assumed that $H > h$, which asserts, that yielding begins at the 1–2 interface and propagates toward the 2–3 interface. Here $\phi = H/h$. When $\phi = 1$, Equation (8.1) reduces to Equation (6.3). If we define ϕ in terms of ς and $\eta(\phi = \varsigma/\eta)$ and then let η approach zero, Equation (8.1) also yields the fully plastic solution for the bi-layer (Suresh et al., 1994).

Figure 5a contains a plot of the yielding sequence for case A as a function of $h/t = H/t$ for $E_1/E_2 = 3$. In this case, a three layered material with complete symmetry, yielding always begins ahead of the crack tip. Next comes the development of plasticity in the wake of the crack-tip at the 1–2 interface. Lastly, plasticity in the wake of the crack-tip propagates from the 1–2 interface to the crack surface.

For Case B, $|\Delta T_{\text{onset}}| = |\Delta T^B_{2-3}|$ and further temperature change results in the spread of plasticity from the 2–3 interface to the 1–2 interface ahead of the crack-tip. $|\Delta T_{FP}| = |\Delta T^B_{FP}|$ is given by:

$$\frac{|\Delta T^B_{FP}(\alpha_3 - \alpha_2)|E_2}{\sigma_{o2}} = \frac{1}{Z\eta}\left(\frac{D^B_1 + D^B_2}{D^B_3 + D^B_4 + D^B_5}\right)\,,$$

[2]For Case A, (i)–(iii) occur when $H > h$. When $H = h$ yielding occurs uniformly ahead of the crack tip and only (ii) and (iii) apply.

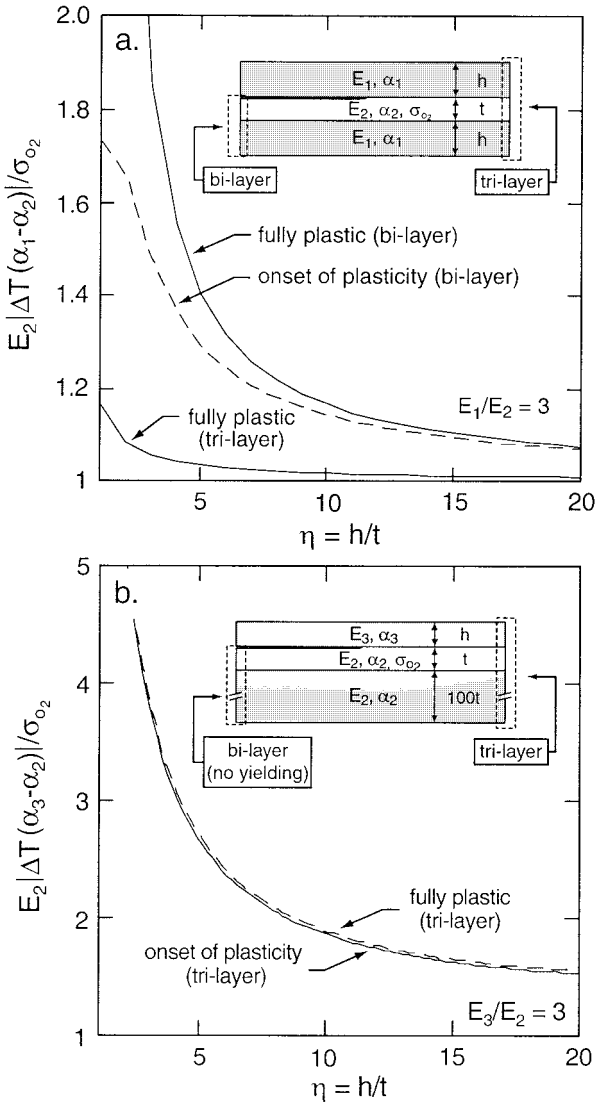

Figure 5. The yielding sequence: (a) Case A with geometric symmetry and (b) Case B with $H/t = 100$ (no yielding in the bi-layer at the crack wake).

$$
\begin{aligned}
D_1^B &= \tfrac{1}{3}(Z\eta + \varsigma + 1)\left(Z\eta^3 + 3Z\eta^2 + \varsigma^3\right), \\
D_2^B &= \tfrac{1}{4}\left(-Z\eta(\eta+2) + \varsigma^2\right)\left(Z\eta^2 + 2Z\eta - \varsigma^2 + 1\right), \\
D_3^B &= \frac{Z\eta^3}{12}, \quad D_4^B = \eta\varsigma^2\left(\frac{\varsigma}{3\eta} + \frac{1}{4}\right), \quad D_5^B = \frac{\varsigma^2}{2}.
\end{aligned}
\tag{8.2}
$$

Figure 5b contains a plot of the normalized $|\Delta T_{(\text{onset})}|$ and $|\Delta T_{FP}|$ temperatures as a function of h/t for $H = 100t$ and $E_3/E_2 = 3$. The close proximity of the two lines indicates that the temperature change required to go from an elastic solution to a fully plastic solution is very small due to the high thickness of the substrate ($100t$).

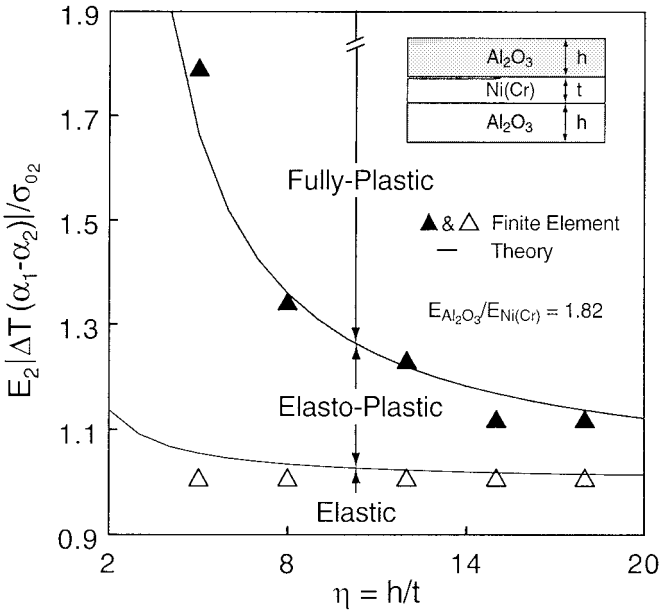

Figure 6. Nominal yielding characteristics of a symmetric tri-layer with elastic-perfectly plastic sandwich layer. Finite element results validate the analytical expressions.

In summary, nominal yielding for Case A always starts in the tri-layer ahead of the crack tip at $|\Delta T_{\text{onset}}| = |\Delta T^{A}_{1-2}|$ (assuming $X > 1, \zeta > 1$, and $H > h$). Once this temperature is reached, G is no longer valid. Figure 6 illustrates the three temperature regimes of interface fracture for the Al_2O_3/Ni(Cr)/Al_2O_3 tri-layer with $H = h$ discussed in the sections that follow. The curve separating the elastic and elasto-plastic solutions is $|\Delta T^{A}_{1-2}|$ for the tri-layer and the curve separating the elasto-plastic and fully plastic solutions is the critical temperature where full plasticity commences in the bi-layer crack wake. The symbols represent finite element results for $\eta = h/t = 5$, 8, 12, 15, and 18.

In the fully plastic regime, the J-integral has an approximate analytical solution when layer 2 is elastic-perfectly plastic, ΔT is uniform, and there is no contact in the wake of the crack. Under these conditions, Equation (3.1) can be approximated as in Olsson and Giannakopoulos (1997), provided that proportional stressing occurs around the crack-tip. For Case A with $H = h$, the fully plastic solution corresponds to

$$J_{FP} = \frac{(\sigma_{o2})^2 t}{4E_2\eta^3 X}(7\eta^2 + 12\eta + 6) \quad \text{(symmetric tri-layer)} . \tag{8.3}$$

This equation was derived from Equations (4.3), (6.3) and (7.1). For the fully plastic bi-layer (Olsson and Giannakopoulos, 1997):

$$J_{FP} = \sigma_{o2}\Delta T(\alpha_2 - \alpha_1)t - \frac{t(\sigma_{o2})^2}{2E_2}\left[1 + \frac{1}{X\eta}\left(\frac{3}{\eta^2} + \frac{6}{\eta} + 4\right)\right] \quad \text{(bi-layer)} . \tag{8.4}$$

Note that unlike Equation (8.4), Equation (8.3) is not influenced by temperature change above ΔT_{FP}. This 'plateau' in the driving force with respect to temperature change means that for the symmetric tri-layer, the J-integral can reach an absolute maximum.

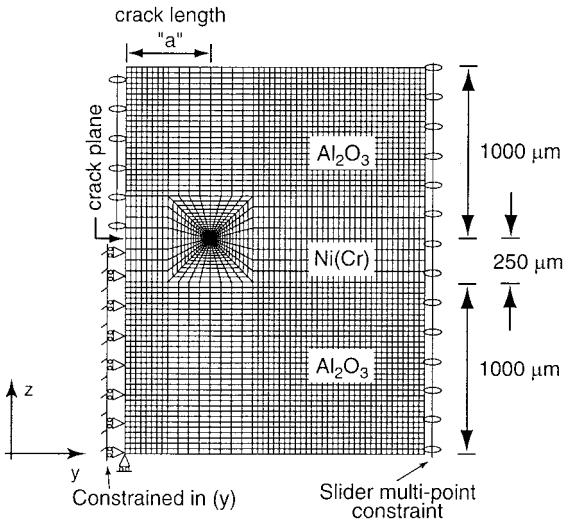

Figure 7. The refined finite element mesh used to calculate crack tip fields and assess the J-integral. The smallest element around the crack-tip was 0.625 μm in length.

9. Finite element results

Equation (3.10) along with conventional elastic stress analysis have provided analytical expressions for G, Equations (4.2)–(4.6). Combined with analytical expressions for the fully plastic J-integral, Equations (8.3) and (8.4) give upper bounds for the interface energy release rate. The region between these bounds, must be described by an elasto-plastic regime. Since there is no analytical solution for this regime, representative results have been obtained using finite element analysis.

Two finite element models have been used in this investigation. The first model consisted of 600, 8-noded plane stress elements arranged in four columns following the lines of Olsson and Giannakopoulos (1997). This model was used to evaluate the far-field J-integral. The second model consisted of approximately 4500, 8-noded plane stress elements with an overall geometry illustrated in Figure 7. The refined mesh in the vicinity of the crack tip for this model allowed for the evaluation of J along several contours near the crack-tip. The J-integral was evaluated using the intrinsic contour integral routine in ABAQUS Version 5.7 (ABAQUS, 1997). Periodic boundary conditions were imposed in front of and behind the crack tip such that beam kinematics hold for the far-field deformation.

9.1. J-INTEGRAL CALCULATIONS IN THE ABSENCE OF CONTACT

This section contains results obtained from the first finite element model that accounts only for the far-field deformation with the J-integral evaluated along a far-field contour. Contact is not considered in this section. Material properties used in the model are given in Table 1. In this case, the thermo-mechanical properties were kept constant with temperature (the finite element code can allow for temperature dependent properties). If the material properties vary only moderately over the temperature range of interest, then temperature-averaged properties could also be used to provide more accurate results (Olsson and Giannakopoulos, 1997). Similarly, plane strain and generalized plane strain can also be modeled within this code.

Table 1. Material properties used in the finite element model.

Material	E (GPa)	ν	σ_o (MPa)	α ($\times 10^{-6}$/°C)
Al_2O_3	378	0.25	–	6.2
Ni(Cr)	208	0.31	330	13.3

Figures 10 and 11 contain numerical results for a symmetric Al_2O_3/Ni(Cr)/Al_2O_3 tri-layer (Case A: $H = h$) subjected to monotonic cooling. The figures truncate at $|\Delta T| > 600$; after that creep would relax stresses in the Ni(Cr) layer[3]. In each figure, J-integral vs. ΔT is plotted and the temperature regimes of interface fracture are distinguished.

The results presented in Figures 8a and 8b are for the same tri-layer with two different values of t, 500 and 250 μm, respectively. When $t = 500$ μm, cooling in the range $0 < |\Delta T| < 600$ °C is not enough to fully yield the bi-layer in the wake of the crack. As a result, J_{FP} is not reached and therefore only the elastic and elasto-plastic temperature regimes are present. The deviation from a linear elastic solution occurs at $|\Delta T| = 255$ °C, which is consistent with the onset of uniform yielding far ahead of the crack tip, Equation (6.3). The limiting elastic energy release rate at which this occurs is consistent with the predictions of Equation (7.1). When the thickness of layer 2 is reduced from 500 to 250 μm, both t and $\eta = h/t = H/t$ change. The net effect is a reduction in the yielding temperatures and a reduction in the plateau value of J as given by Equation (8.3). For this geometry, the elastic solution, $J = G$, is valid up to $|\Delta T| = 247$ °C. The fully plastic plateau is reached at $|\Delta T| = 427$ °C with a plateau value equal to 48 J m^{-2}. Thus the finite element model captures the trends predicted by Equation (8.3).

Comparing the two configurations shown in Figure 8, four important results are apparent. First, the elastic energy release rate significantly overestimates the elasto-plastic J for $|\Delta T| > |\Delta T_{\text{onset}}|$. Second, by reducing the thickness of layer 2, the energy release rate reduces dramatically. This attests for the strong dependence of J on geometry. Third, the interlayer yield strength, σ_{02}, plays an important role in determining J through both the scaling of the temperature bounds and the magnitude of J_{FP}. Fourth, the temperature regimes depicted in Figure 6, based on far-field nominal yielding, also capture the transition temperatures observed for the changes in the J-integral.

Figures 10a and 10b have shown results for the case when layer 2 is elastic-perfectly plastic. If layer 2 is capable of strain hardening, the plateau in J is not reached. Figure 9a shows how J changes as a result of moderate linear strain hardening defined by a tangent modulus (H_T) equal to 1%, 5%, and 20% of the elastic modulus E_2. The small change in J for $H_T = 0.01E_2$ and $0.05E_2$ suggests the elastic-perfectly plastic solution can still modestly predict the response of materials which exhibit low strain hardening, e.g., pure annealed FCC metals.

Figure 9b shows the evolution of J with temperature for an Al_2O_3/Ni(Cr) bi-layer obtained by setting $H = 0$. The shaded region in the bottom of the figure marks the area which completely bounds the solution for a tri-layer that can be formed if an additional 1000 μm

[3]Creep is important for temperatures higher than the homologous temperature, 0.5. For Ni(Cr)$T_M = 1390$ °C.

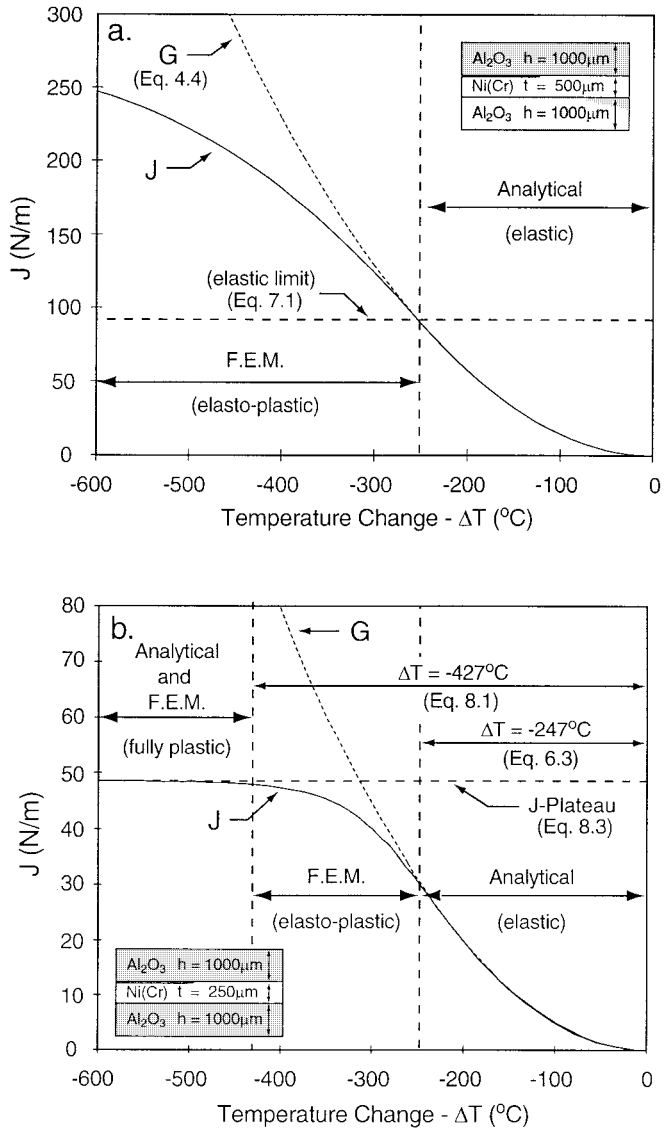

Figure 8. J vs. Temperature curves for an Al_2O_3/Ni(Cr)/Al_2O_3 tri-layer: (a) with $t = 500$ μm and (b) with $t = 250$ μm. $H = h = 1000$ μm in both subfigures.

layer of Al_2O_3 is applied to the Ni(Cr). Note that the bi-layer and the tri-layer in Figure 9b have the same $|\Delta T_{FP}|$. A comparison of Figures 10b and 11b shows the two central differences between these solutions. First, the driving force, J, for interface fracture is higher in the bi-layer than it is for the equivalent symmetric tri-layer. Second, the difference between the elastic, G, and elastic-plastic, J, is much more pronounced for the tri-layer. The latter indicates the advantage of having plasticity develop and spread both in the wake and ahead of the crack tip.

Finite element results representative of Case B are shown in Figure 10. In this example layers 1 and 2 have the elastic properties of Ni(Cr) and layer 3 has the properties of Al_2O_3. The interlayer (layer 2) has been given a very small yield strength, $\sigma_{o2} = 20$ MPa, in order

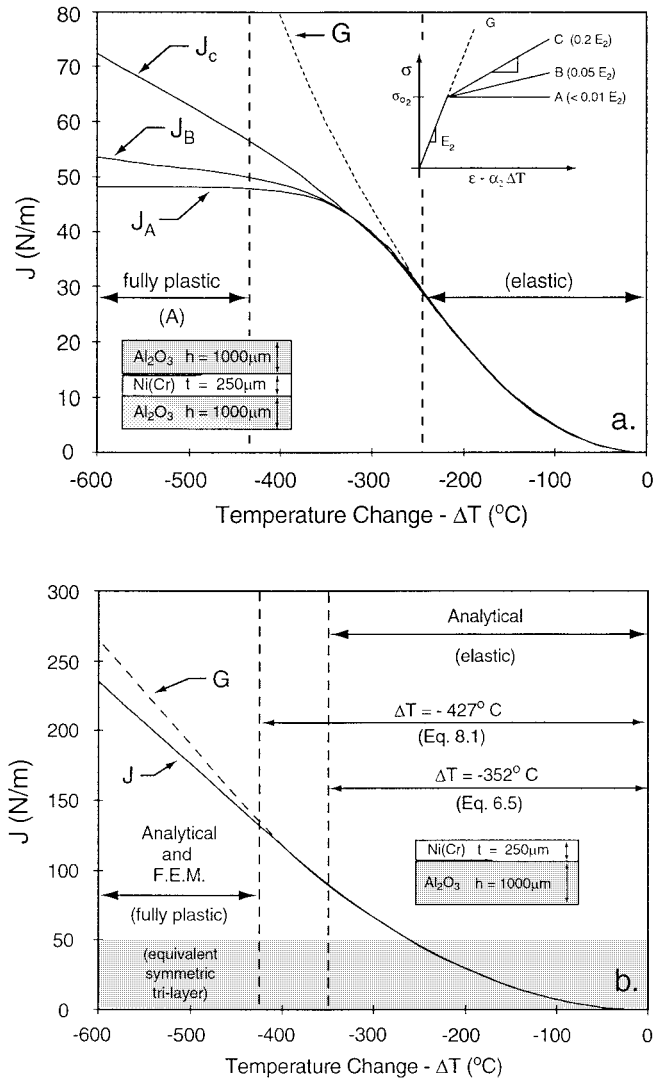

Figure 9. (a) The influence of strain hardening on $J(\Delta T)$ and (b) $J(\Delta T)$ for a bi-layer with no strain hardening.

to accentuate results in the fully plastic regime. Since layers 1 and 3 remain elastic, plastic deformation remains confined within layer 2.

Equations (4.4), (8.4) and (8.3) show that the energy release rate under thermal loading has either second, first, or zeroth-order dependence on ΔT : $G \propto \Delta T^2$, $J_{FP} \propto \Delta T$ for the bi-layer and $J_{FP} \propto \Delta T^0$ for the tri-layer.

9.2. Path-dependence of the J-integral and alternate stress states

The analytical derivations and finite element results up to this point are valid for plane stress. This section considers alternate stress states and their influence to the path dependency of the J-integral in the elasto-plastic and fully plastic regimes. In order to do this, the second finite element model, having a refined mesh in the vicinity of the crack, was used. As a means of comparing near-tip and far-field values, the J-integral was evaluated along fifty concentric

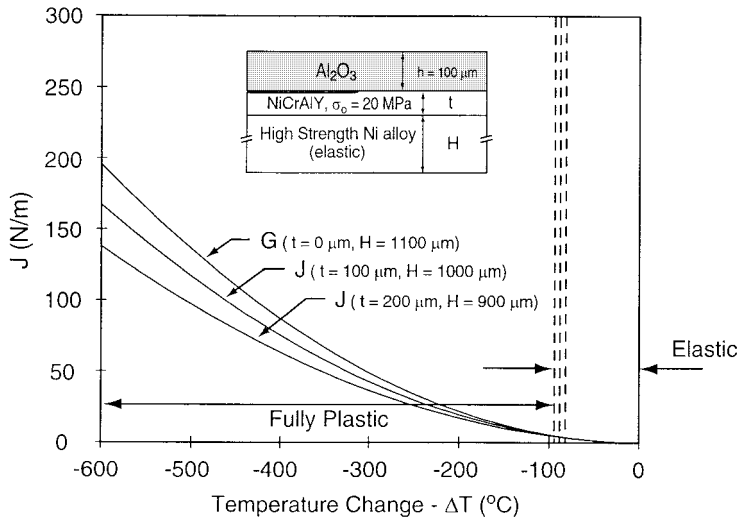

Figure 10. J vs. Temperature curves for Case B using properties of Ni(Cr) and Al_2O_3.

circles having origins centered at the crack tip and radii ranging from $y/t = 0.0025$ to $y/t = 1$ (Figure 1). For plane stress, results from the latter were in exact agreement with those obtained along the far-field contour discussed in Section 9.1.

In order to limit the scope only representative solutions for the Al_2O_3/Ni(Cr)/Al_2O_3 tri-layer (Case A) with $t = 250$ μm and $H = h = 1000$ μm are discussed. Figure 11 contains plots of the J-integral vs. ΔT evaluated along a far-field path ($y/t = 1$) and near-tip path ($y/t = 0.0025$). Results for plane stress, plane strain and generalized plane strain are presented. In each case, a small amount of strain hardening, defined by a linear tangent modulus, H_T, was added to facilitate numerical convergence. J_{FP} based on plane stress has been plotted in each figure for comparison. When modeling the generalized plane strain state, the uncracked ligament w was varied from 4 to 8 times the crack length, a, in order to determine the dependence of J on model length[4]. This procedure indicated that beyond $w = 5a$ there was negligible effect of w on J. The presented results are for $w = 5a$.

Figures 13a and 13b illustrate two points. First, when $y/t = 1$, the generalized plane strain and plane stress solutions have similar values, both being approximately equal to J_{FP} in the fully yielded regime. The plane strain solution lies significantly below these two because the additional out-of-plane constraint reduces $|\Delta T|$ for both yield initiation and full plasticity. Second, the near-tip $J(y/t = 0.0025)$ for all stress states deviates from the far-field J.

The plane strain state, though modeled here, is not appropriate for the present thermal problem since it over-constrains the tri-layer (Gaudette et al., 1997). Thus the deviation from J_{FP} for this stress state is not a significant source for concern.

Figure 12 contains plots of the stress fields ahead of the crack tip for the generalized plane strain and plane stress states for the Al_2O_3/Ni(Cr) tri-layer with $t = 250$ μm and $H = h = 1000$ μm. The evolution of these fields, particularly σ_{yz} and σ_{zz}, in plane stress and generalized plane strain respectively, for $|\Delta T| > |\Delta T_{FP}^{\text{bi-A}}| = 427$ °C, suggests that the single parameter characterization of cracking along the interface is breaking down. The normalization used for both the ordinate and abscissa in Figures 12a and 12b is such that the normalized stress

[4]The overall model length ($a + w$) must resemble an edge crack in a semi-infinite slab. For generalized plane strain the length w influences the out-of-plane constraint for $y < 0$.

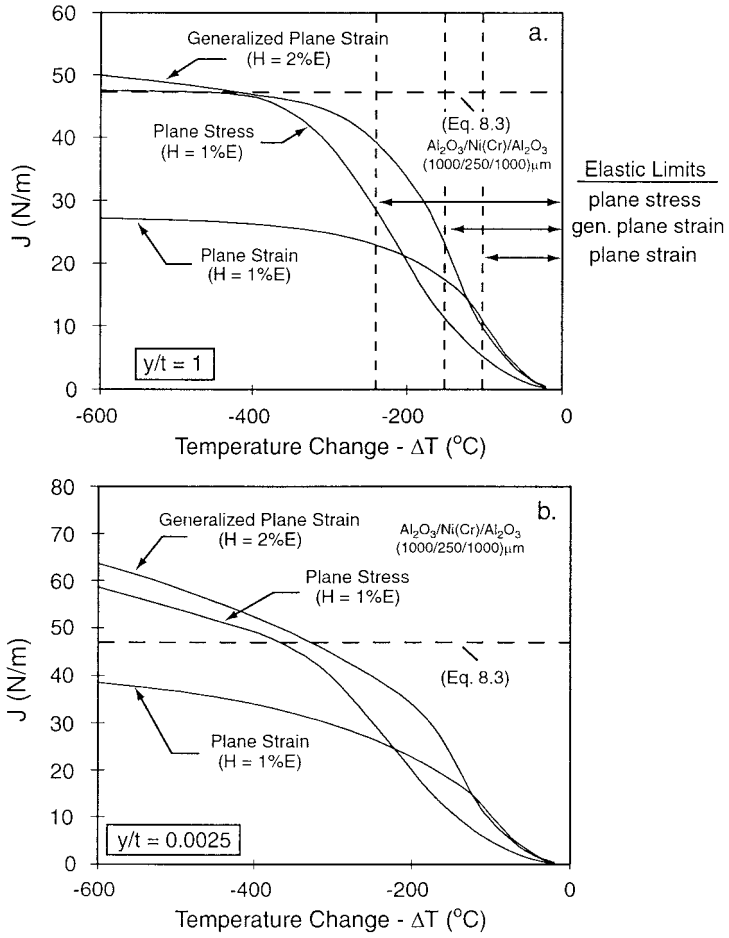

Figure 11. The (a) far-field ($y/t = 1$) and (b) near-tip ($y/t = 0.0025$) J for plane stress, plane strain and generalized plane strain ($t = 250\ \mu$m, $H = h = 1000\ \mu$m).

fields would have been invariant with temperature, if a single parameter characterization of the crack-tip existed. Additional parameters to the J-integral may be the hydrostatic stress state or the T-stress at the crack-tip (O'Dowd and Shih, 1991). For generalized plane strain the stress fields ahead of the crack tip can be approximated as

$$\sigma_{yz} \approx \frac{K_{II}/\sqrt{J_{\text{tip}}/\sigma_{02}}}{\sqrt{2\pi y/(J_{\text{tip}}/\sigma_{02})}}, \quad 2 \le \frac{y}{J_{\text{tip}}/\sigma_{02}} \le 5\ ,$$
$$\sigma_{zz} \approx \frac{K_I/\sqrt{J_{\text{tip}}/\sigma_{02}}}{\sqrt{2\pi y/(J_{\text{tip}}/\sigma_{02})}} + Q, \quad 2 \le \frac{y}{J_{\text{tip}}/\sigma_{02}} \le 3, \tag{9.1}$$

where, for the tri-layer, Q is approximated by

$$Q \approx 2\frac{(\alpha_2 - \alpha_1)\Delta T t}{2h/E_2 + t/E_1}\ . \tag{9.2}$$

For the example in Figure 12b, $K_{II}^2/J_{\text{tip}} = 16.6$ GPa.

Furthermore, Figure 12c suggests that this stress-state may influence the fracture characteristics of these interfaces through the phase between normal and tangential loading, $\Psi =$

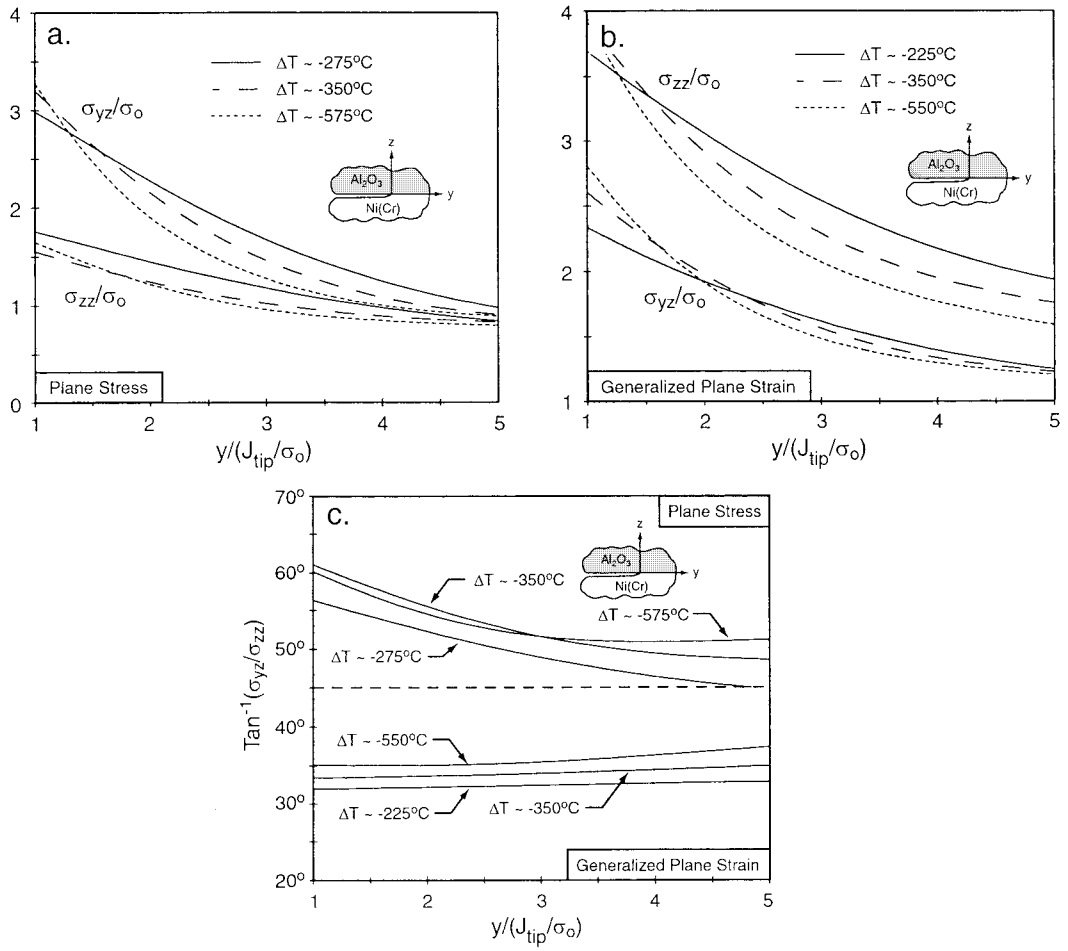

Figure 12. Near-tip stress fields ($t = 250\ \mu$m, $H = h = 1000\ \mu$m): opening and shear mode stress for (a) plane stress and (b) generalized plane strain and (c) loading phase, $\Psi = \tan^{-1}(\sigma_{yz}/\sigma_{zz})$

$\tan^{-1}(\sigma_{yz}/\sigma_{zz})$. This figure demonstrates that Ψ for generalized plane strain is significantly lower than it is for plane stress. However Ψ varies mildly with position for the generalized plane strain, in comparison with the plane stress case.

The findings shown in Figures 12a–c are typical of the large-scale yielding conditions that develop in the fully plastic regime. One consequence is that J may be more configuration dependent (and deviate from the estimate given in Equation (8.3)) as plasticity propagates through the layers (Anderson, 1991). Likewise, a failure or growth criterion may also have to take into account this dependency (McClintock et al., 1995). Despite these findings, it is believed that J_{FP} still remains a better approximation than G. For the case of the Al_2O_3/Ni(Cr)/Al_2O_3 tri-layer with $t = 250\ \mu$m $G = 177, 334$, and 371 J m^{-2} for plane stress, generalized plane strain and plane strain, respectively. The latter value, though obtained from the finite element model, could be calculated by substituting $E_i \rightarrow E_i/(1 - v_i^2)$ and $\alpha_i \rightarrow \alpha_i/(1 + v_i)$ into Equation (4.4), as suggested in (Suresh et al., 1994). Furthermore, the analytical solution J_{FP} provides a convenient and quick starting place for more detailed analysis.

The preceding analysis assumed that the crack is stationary and remains at the interface. Though interface crack growth is not addressed in this paper it is important to note that a crack initiating at an interface may not necessarily propagate along the interface. The preferred growth direction depends on the ratio of the interface toughness to the toughness of the adjoining layer as well as their stiffness ratio, as noted in (He and Hutchinson, 1989; Simonov, 1992). For the Al_2O_3/NiCr example given above the interface crack will tend to propagate along the interface because the interface toughness is less than $\sim$0.5 the toughness of the Ni(Cr). For values greater than this the interface crack will kink into the Ni(CR) and blunt. Further details can be found in (Gaudette, 1999).

9.3. Interfacial contact

The contact model presented in Section 5 predicts that large scale contact in the wake of the interface crack reduces the driving force for interface fracture. In this section results from finite element simulations that include contact are presented. The finite element model used the refined mesh (Figure 7) with frictionless contact elements added along the whole interface between layer 3 and 2 over the entire length ($-a < y < 0$). Figures 13a and 13b contain results for a Ni(Cr)/Al_2O_3 tri-layer with $t = 250$ and $H = h = 1000$ μm under conditions of plane stress. In Figure 13a, elastic conditions are assumed for direct comparison with the results from the contact model shown in Figure 3. Plotted in Figure 13a are the finite element solutions with and without contact constraint, as well as the analytical solution predicted by Equation (5.8). Figure 13b contains elastic-plastic results for the Ni(Cr) tri-layer with $H_T = 0.01E_2$.

Under elastic conditions the finite element model predicts a contact shielding effect of $\sim$26%. This value agrees quite well with the value 22% predicted from Equation (5.8). Additional model results further confirm two other theoretical results: (i) the shielding affect as a percent of G is nearly constant and (ii) a single point is in contact in the crack wake. The localization of contact in the vicinity of $y = -a$ is consistent with the single point result used in the analytical contact model. Further, the finite element analysis did not reveal any local crack closure at the crack-tip, as plasticity resulted in significant crack-tip blunting.

During cooling, yielding in the Ni(Cr) causes J to deviate from G. With contact, the deviation is further enhanced as additional strain energy builds up in the crack wake. These trends are demonstrated in Figure 13b. The 'predicted J' shown in the figure was obtained by extending the elastic analysis correction obtained from Equation (5.8) to J_{FP}, obtained from Equation (8.3). Such extension gives an *approximate* analytical expression for the far-field J in the presence of contact.

10. Discussion of results

The present work has examined the evolution of the energy release rate, the J-integral, for a stationary crack in a three-layered metal–ceramic system subject to monotonic thermal loading. For a plane stress state with incremental thermo-elasto-plasticity, analytical expressions for the deformation and the energy release rate were derived. In addition, finite element calculations confirming the analytical expressions were carried out.

The overall behavior of the composite was found to depend on characteristic temperatures which mark the bounds between the three regimes of interface fracture; elastic, elasto-plastic, and fully plastic. For interfaces that debond at a critical value of J, the results of this paper

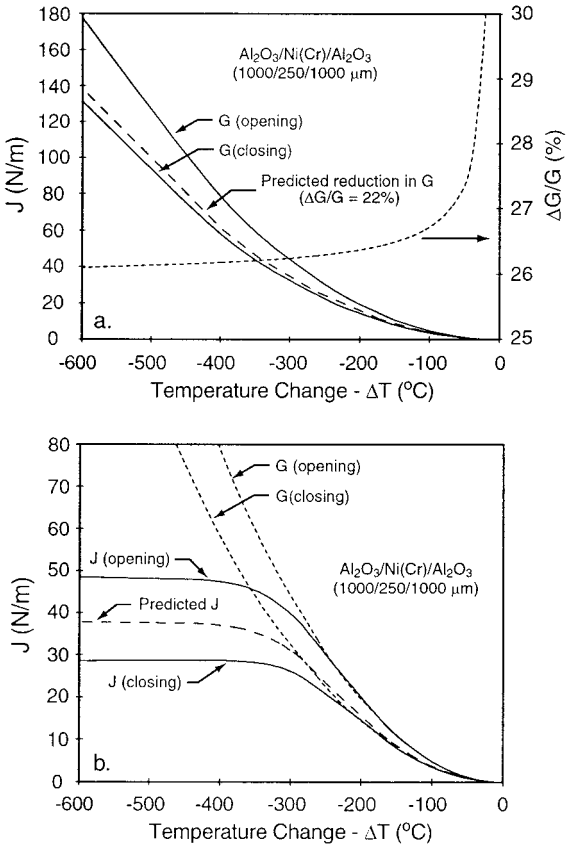

Figure 13. Finite element simulations of large-scale interfacial contact in the wake of an interface crack ($t = 250\ \mu$m, $H = h = 1000\ \mu$m): (a) elastic conditions for comparison with the contact model and (b) elastic-plastic conditions for the Ni(Cr) tri-layer.

may be used to define the characteristic temperature at which growth of an edge-crack may initiate.

This work has been concerned with three layered material systems. In some instances assumptions regarding the material behavior of the layers have been made for purposes of simplification. In spite of this, the adopted solution procedure is general in the sense that it can be applied to many layered material systems with each layer having unique thermal, elastic and plastic properties. Besides thermal strains, other eigenstrains such as sintering and moisture swelling can be dealt with in a similar way.

The most important features identified in this work relate to the interacting roles of plasticity, geometry, and large-scale contact. It has been shown that each of these features plays a role in determining J. If a layered material can be designed with low characteristic temperatures, $|\Delta T_{\text{onset}}|$ and $|\Delta T_{FP}|$, it can benefit substantially from the shielding effects of plasticity. Furthermore, if a layered system also utilizes an optimized geometry, additional benefits can be realized. Case A with $H = h$ is an example. By reducing the thickness of layer 2, both $|\Delta T_{\text{onset}}|$ and $|\Delta T_{FP}|$ are reduced. At the same time, by making the geometry symmetric, the additional benefit of a limit J was obtained.

The development of plasticity across the entire interface and ahead of the interface crack-tip, for $|\Delta T| > |\Delta T_{\text{onset}}|$, leads to large-scale plasticity effects in fracture. This branch of

fracture mechanics is notorious for the scarcity of analytical results, as well as the breakdown of the path-independence of line integrals used to characterize non-linear elastic fracture (Olsson and Giannakopoulos, 1997). If the energy release rate, J, were to be used against interface fracture initiation in thermally loaded layered materials, the following points have to be considered:

(i) The crack driving force, as given by the J-integral, does not depend on crack length provided that the crack is longer than the largest layer thickness.

(ii) The J-integral can be approximated by a far-field line integral in the elastic and elasto-plastic regime.

(iii) The J-integral can take into account the effects of large-scale contact in the elastic regime. An elastic contact model provides a closed-form solution which predicts how contact reduces the energy release rate.

(iv) The J-integral is strongly dependent on material properties, layer thickness, and configuration.

(v) The J-integral has to be supplemented with some measure of the mode mixity and the hydrostatic stress state close to the crack-tip.

Acknowledgements

The work was supported by a MRSEC Grant DMR 9632570 from the National Science Foundation, which was funded at MIT as a subcontract through the Center for Thermal Spray at the State University of New York, Stony Brook.

References

ABAQUS version 5.7 (1997). Hibbitt, Karlsson and Sorensen Inc., Pawtucket, R.I.

Anderson, T.L. (1991). Fracture mechanics. *Fundamentals and Applications*. CRC Press, Boca Raton, FL, 179.

Bogy, B. (1971). Two edge bonded elastic wedges of different materials and wedge angles under surface tractions. *ASME Journal of Applied Mechanics* **38**, 377–386.

Beuth, J.L. and Narayan, S.H. (1996). Residual stress-driven delamination in deposited multilayers. *International Journal of Solids and Structures* **33**, 65–78.

Cao, C., Thouless, M.D. and Evans, A.G. (1988). Residual stresses and cracking in brittle solids bonded with a thin ductile layer. *Acta Metallurgica et Material* **36**, 2037–2046.

DiSciuva, M., Icardi, U. and Librescu, L. (1999). Effects of interfacial damage on the global and local static response of cross-ply laminates. *International Journal of Fracture* **96**, 17–35.

Gaudette, F. (1999). Ph.D. Dissertation, MIT, Cambridge, MA 02139.

Gaudette, F., Suresh, S., Evans, A.G., Dehm, G. and Rühle, M. (1997). The influence of chromium addition on the toughness of γ-Ni/α-Al_2O_3 interfaces. *Acta Metallurgica et Materialia* **45**, 3503–3513.

He, M.Y. and Evans, A.G. (1991). The strength and fracture of metal/ceramic bonds. *Acta Metallurgica et Material* **39**, 1587–1593.

He, M.Y. and Hutchinson, J.W. (1989). Kinking of a crack out of an interface. *Journal of Applied Mechanics* **56**, 270–278.

Hutchinson, J.W. and Lu, T.J. (1995). Laminate delamination due to thermal gradients. *ASME Journal of Engineering Materials and Technology* **117**, 386–390.

Kuo, Y. (1989). Thermal stress at the edge of a bimetallic thermostat. *ASME Journal of Applied Mechanics* **56**, 585–589.

McClintock, F.A., Kim, Y.-J. and Parks, D.M. (1995). A criterion for plane strain, fully plastic, quasi-steady crack growth. *International Journal of Fracture* **72**, 197–221.

Nakamura, T. (1991). Three-dimensional stress fields of elastic interface cracks. *ASME Journal of Applied Mechanics* **58**, 939–946.

O'Dowd, N.P. and Shih, C.F. (1991). Family of crack-tip fields characterized by a triaxiality paramter: Part I – Structure of fields. *Journal of Mechanics and Physics of Solids* **39**, 989–1015.

Olsson, M. and Giannakopoulos, A.E. (1997). Elasto-plastic analysis of layered materials under thermal loading: edge cracks parallel to the interface. *International Journal of Fracture* **85**, 81–97.

Shen, Y.L. and Suresh, S. (1995). Elasto-plastic deformation of multi-layered materials during thermal cycling. *Journal of Materials Research* **10**, 1200–1215.

Simonov, I.V. (1992). Prediction of arbitrary crack growth from the interface between two dissimilar elastic materials. *International Journal of Fracture* **57**, 349–363.

Suo, Z. and Hutchinson, J.W. (1990). Interface crack between two elastic layers. *International Journal of Fracture* **43**, 1–18.

Suresh, S., Giannakopoulos, A.E. and Olsson, M. (1994). Elasto-plastic analysis of thermal cycling: layered materials with sharp interfaces. *Journal of Mechanics and Physics of Solids* **42**, 979–1018.